Hindawi
Shock and Vibration
Volume 2019, Article ID 1659175, 15 pages
https://doi.org/10.1155/2019/1659175

Research Article

Experimental Study and Numerical Simulation of Dynamic Stress-Strain of Directional Blasting with Water Jet Assistance

Dengfeng Su,[1] **Dandan Zheng**,[2] **and Lingang Zhao**[1]

[1]*School of Environment and Resource, Southwest University of Science and Technology, Mianyang 621010, China*
[2]*Dazhou Administration of Work Safety, Dazhou 635000, China*

Correspondence should be addressed to Dengfeng Su; dengfengcqu@163.com

Received 2 November 2018; Revised 7 January 2019; Accepted 19 February 2019; Published 24 March 2019

Academic Editor: Adam Glowacz

Effective control of the explosive energy and the propagation direction of blast-induced crack and minimizing damage of remaining rock mass are the main purposes of directional-controlled blasting. In this paper, the experimental test on blast strain fields affected by water jet slot and blasthole wall protection material is conducted. Next, the FEM software ANSYS/LSDYNA is used to simulate the blast-induced crack propagation and the blast stress wave transmission of different types of blasthole, and the distribution and evolution law of dynamic blast stress are also analyzed. The results indicate that the existence of blasthole wall protection material is not only beneficial to the "guiding effect" of blast-induced crack propagation of water jet slot but also beneficial to reduce blast-induced damage of remaining rock mass. Besides, the bigger D_m/r_b is, the weaker the "guiding effect" and "blasthole wall protection effect" by water jet slot and wall protection material are.

1. Introduction

In China, drill-blasting method is the most cost-effective way in the construction of underground space engineering. However, it has many disadvantages, which produces some random radial fractures from a blasthole along the unspecific directions and invites overbreaks among the rock masses with low strength or with a number of cracks, posing a serious threat to long-term stability of permanent structures including underground nuclear waste repositories and open-pit slopes [1]. To solve the disadvantages of the traditional drill-blasting method, directional control blasting technology was put forward, and its main purpose is effective control of the explosive energy and the propagation direction of the blast-induced crack [2, 3]. The most direct ways to guide crack growth along the specific direction and inhibit crack growth along other directions are to make notches by using grooving machine along the desired direction on the surface of the borehole wall [4–6]. Based on this idea, several researchers [7–10] have done many researches for guiding crack propagation and minimizing rock damage in the undesired directions so as to achieve better performance of fracture plane control, and many works investigated the notched borehole blasting technique with different solutions. Katsuyama et al. [11] suggested a controlled blasting method using a sleeve with slits in a borehole. Fourney et al. [12, 13] conducted controlled blasting experiments with a notched borehole in PMMA specimens, which demonstrated that blast-induced crack propagated along the notched direction under the blast loading. Mohanty [14, 15] suggested a fracture plane control technique using satellite holes on either side of the central pressurized hole and demonstrated its use through laboratory experiments and field tests in rock. Du et al. [16] studied the mechanical effect of the V-shape notched borehole under the blast loading, and the control mechanism of the notch to rock-oriented cracking is demonstrated, and the criterion for the advance on initial crack in notched borehole blasting is established. Zong [17, 18] analyzed the beginning and end condition as well as the developing direction, speed, and length when decoupling charge is adopted for symmetric grooved hole well based on the theory of rock fracture mechanics and function of explosion gas. Cho et al. [19] proposed a dynamic fracture process analysis based on the dynamic finite element method and fracture mechanics to verify the dynamic

fracture and fragmentation mechanism due solely to the stress wave in blasting. Zhang [20] simulated the stress distribution law by ANSYS/LS-DYNA, and the dynamic seam forming mechanism is also analyzed based on the fracture mechanics theory. Yang et al. [21, 22] studied the crack propagation and changes in stress intensity at the crack tips of the two V-notched borehole by the blast loading system using dynamic reflected caustics. The experimental results show that the crack tips do not meet directly but are deflected and become anisotropic, and the crack propagation velocity first decreases, oscillates, and then gradually increases to peak followed by a decrease until the oscillations stop. Yue et al. [23, 24] conducted model experiments to investigate the influence of empty holes with different shapes on directional fracture-controlled blasting of rock by using new digital laser dynamic caustics. The results show that the preset rhombic hole can achieve fine directional fracture-controlled blasting and effectively ensure the forming effect of blasting around the roadway. Chen et al. [25] analyzed the mechanism of rock fracturing between holes in deep-hole presplit blasting and the crack evolution under the synergistic action of dynamic and static loads, and the scope of stress-induced cracks around blastholes and the maximum length of secondary cracks induced by detonation gas were calculated. Zhu and Xu [26] compared the stress and damage distribution of conventional circle hole and notch hole by implementing a user-defined statistical damage model based on the secondary development of the LS-DYNA, and the results demonstrate that two mechanical effects are induced by the notch, and high stress concentration is generated at the edge of the notch and the stress at the other part of blasthole is reduced.

Above research studies concentrate mainly on the V-notch directional blasting technology with mechanical grooving tool assistance and demonstrate that this method is superior to the traditional blasting technology to control the direction of blast-induced crack propagation. However, this method has a disadvantage of notching tool to be stuck and wear and tear, especially for the soft surrounding rock blasting. In order to solve this problem, the unique character for low damage, directional control cutting, and highly energy accumulation of water jet attracted the attention of researchers (Figure 1) [27, 28], and then the directional-controlled blasting with water jet assistance was put forward [29–32]. Its mechanism was analyzed and the blast-induced crack initiation criterion along the direction of the water jet slot under blast loading was established. Furthermore, the effect of water jet slot for reducing blast-induced ground vibration in tunnel excavation was analyzed by Kim and Song [30], and the nonlinear hydrokinetics code (AUTODYNA) was used to simulate the effect of reduction of blast-induced vibrations by abrasive water jet cutting.

Based on above studies, an attempt was made in this paper to study the dynamic evolution law of blasting strain under different conditions. An experiment was performed to investigate the evolution law of dynamic strain of different models. Then, numerical simulation for the transmission and reflection of blast stress wave and the propagation law of blast-induced crack were performed by using the FEM software ANSYS/LS-DYNA.

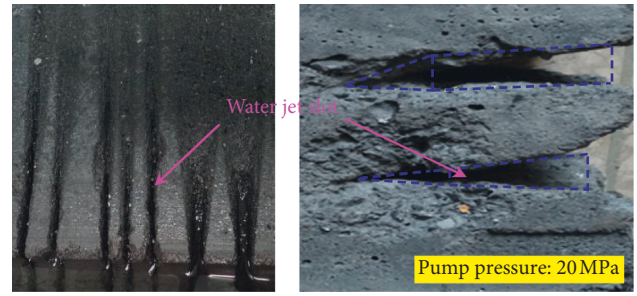

Figure 1: Coal and rock mass cutting using water-only jet.

2. Experimental Test on Dynamic Blasting Strain

2.1. Test Instrument and Test Principle. Blast stress wave has the characteristics of wide band, high upper limit frequency, and large amplitude change, so the test instrument must have a high sampling frequency. In this paper, a multichannel dynamic analysis signal testing system produced by Donghua Testing Technology Co., Ltd., was applied; it comprises an ultrahigh dynamic strain meter with eight channels, a blast loading system, and a computer used to collect blasting data; the connection of the test system is shown in Figure 2, and the procedure of experimental test is shown in Figure 3.

PMMA was used in these blast tests in that it almost shares similar fracture behaviors with brittle rock under dynamic conditions [33]. PMMA specimens were 300 mm × 300 mm × 2 mm in size, and its parameters are shown in Table 1. A blasthole was placed in the center of the specimen, with the center of the blasthole 150 mm from the four sides. All the blastholes are 3 mm in radius.

In order to investigate dynamic strain law under different blasting conditions, three shapes of blastholes were designed: #1 test model has one regular blasthole, #2 test model has one blasthole with two water jet slot along the horizontal axis, and #3 test model has one water jet slotted blasthole with the blasthole wall protection material mounted on the two opposite surfaces of the blasthole; PVC material was used as the wall-protected material. Each test model and its strain gauge arrangement are shown in Figure 4. In addition, each blasthole was charged by 40 mg explosive which was made of propellant, and the spark starter was used as a detonating device.

2.2. Experimental Results Analysis. Table 2 and Figures 5–7 present different types of strain values under three different blasting models, respectively. For #1 test model, mean strain peak value (PSPV) at #E1-1 test point is very close to the PSPV at #E1-3 test point, and the mean strain peak value at four test points is close to the same. In addition, the strain wave evolution law of #E1-1 test point is almost the same as that of #E1-3 test point, and so as to #E1-2 test point and

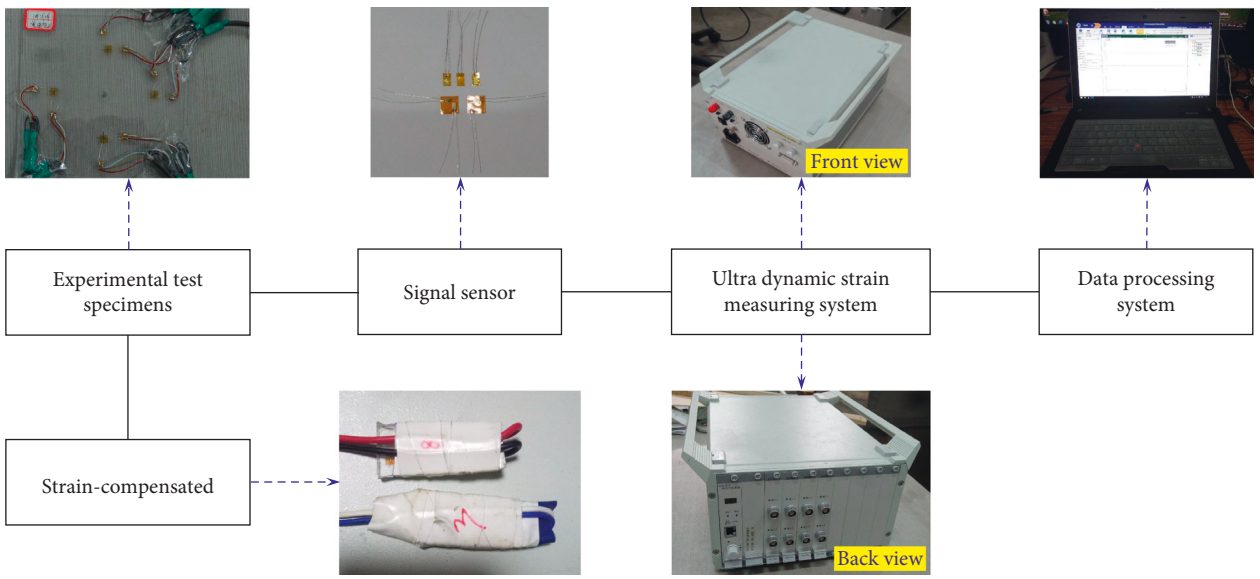

Figure 2: Diagram of test system connection.

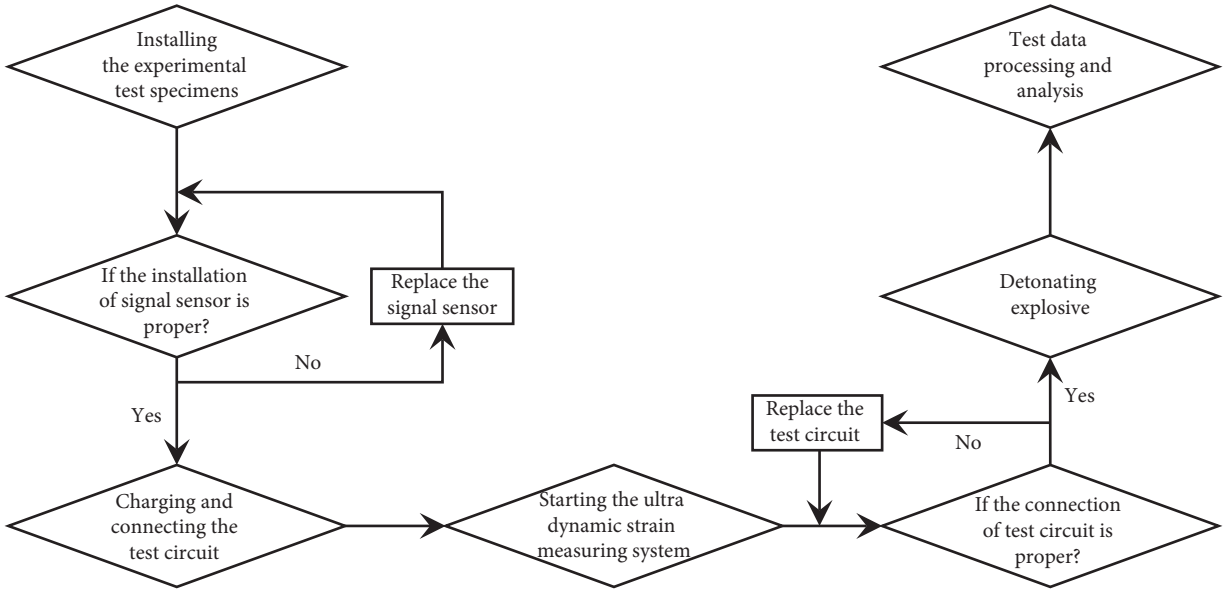

Figure 3: Diagram of experimental test procedure.

Table 1: Parameters of PMMA.

Density (g/cm^3)	Poisson ratio	Elastic modulus (GPa)	Longitudinal wave velocity (cm/μs)	Shear wave speed (cm/μs)
1.2	0.31	6.1	2.3×10^5	1.26×10^7

#E1-4 test point, which shows that when the explosive explodes in a regular blasthole, the blasting load almost evenly works on the circular blasthole surface [34].

By comparing Figure 5 with Figure 6, we can see that the PSPV value at #E2-1 test point is 36.67% greater than PSPV at #E1-1 test point, and the PSPV at #E2-2 test point is 17.9% greater than the PSPV at #E1-2 test point. That is because the water jet slot results in stress concentrations along the direction of the water jet slot while detonation gases work on the blasthole surface or stress waves arrive at the tip of the water jet slot during blasting. In addition, the positive strain peak value (PSPV) and mean strain peak value (MSPV) at #E1-3 test point and #E1-4 test point are almost the same as the PSPV and MSPV at #E2-3 test point and #E2-4 test point and so as to the evolution law of explosive strain wave. It can be seen from the above analysis that the water jet slot changed the law of stress field distribution during the blasting, which results in the stress concentrations

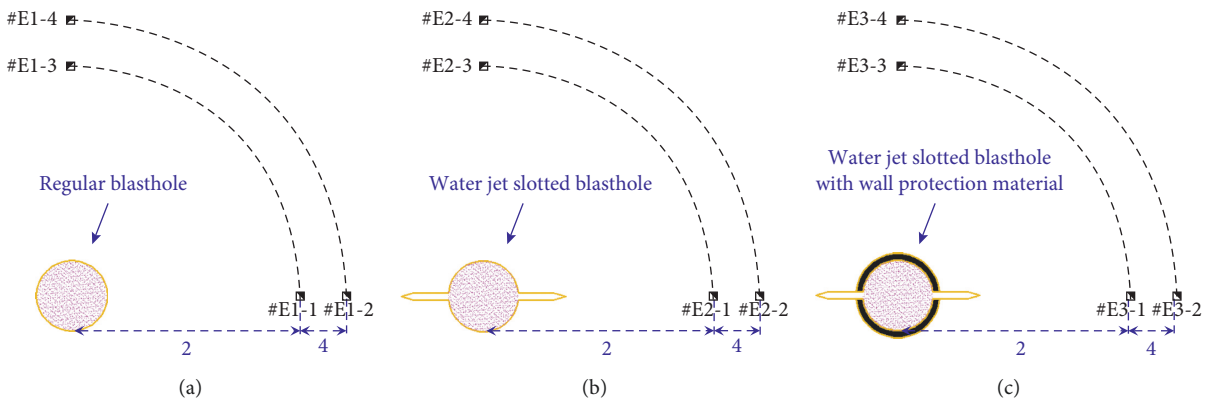

Figure 4: Sketches of three different blasting models and the strain gauge arrangement: (a) #1 test model, (b) #2 test model, and (c) #3 test model.

Table 2: Strain values for three different blasting models.

Test model	Strain value	Values ($\mu\varepsilon$)			
		Channel 1	Channel 2	Channel 3	Channel 4
Model 1	Positive strain peak value	636.454	537.698	672.342	570.690
	Negative strain peak value	−495.945	−248.893	−722.151	−396.569
	Mean strain peak value	83.223	73.074	92.998	78.041
Model 2	Positive strain peak value	869.829	633.962	623.167	520.278
	Negative strain peak value	−341.492	−280.124	−718.531	−388.996
	Mean strain peak value	171.153	132.421	80.121	63.676
Model 3	Positive strain peak value	1177.456	810.468	350.768	295.034
	Negative strain peak value	−772.859	−348.843	−368.530	−271.644
	Mean strain peak value	224.876	189.897	27.480	12.654

along the direction of the water jet slot. However, in the direction perpendicular to water jet slot, the existence of water jet slot has hardly changed the distribution of stress field.

For #3 test model, the existence of blasthole protection material has greatly changed the distribution law and evolution law of the explosive strain wave. On one hand, the PSPV in the direction of the water jet slot gradually increases: the PSPV at #E2-1 test point is 36.67% greater than the PSPV at #E1-1 test point, the PSPV at #E3-1 test point is 35.37% greater than PSPV at #E2-1 test point, and the PSPV at #E3-1 test point is 85.00% greater than the PSPV at #E1-1 test point. On the other hand, the blasting strain values in the direction perpendicular to water jet slot, respectively, decrease to smaller values. Just in regard to the PSPV, the figure (623.167 $\mu\varepsilon$) at #E2-3 test point sees a 43.7% decrease, ending up with 350.768 $\mu\varepsilon$ at #E3-3 test point, and the figures at #E2-4 test point and #E3-4 test point almost share the same decreasing proportion. It is suggested that, in contrast with directional-controlled blasting with water jet assistance, the existence of blasthole wall protection material can sharply reduce the energy of stress wave working on the remaining sides, so as to achieve the purpose of protecting the surrounding rock.

Furthermore, by comparing the blasting strain of #2 test model and #3 test model, we can see that in the direction of water jet slot, the blast strain is much greater than that in the direction perpendicular to water jet slot. For #2 test model, the PSPV at #E2-1 test point sees a 28.36% decrease from 869.829 $\mu\varepsilon$, reaching 623.167 $\mu\varepsilon$ at #E2-3 test point. Besides, for #3 test model, compared with PSPV (1177.456 $\mu\varepsilon$) at #E3-1 test point, the PSPV at #E3-3 test point falls by 70.21%, ending at 350.768 $\mu\varepsilon$. Both the two decreasing trends demonstrate that water jet slot can have an obvious effect on stress concentration along the direction of water jet slot so as to more easily generate perforative fractures along this direction during blasting, and the remaining rock can be better protected.

To sum up, some conclusions can be summarized from the experimental test, as follows:

(1) Under the combined effect of blasthole wall protection material and water jet slot, the PSPV, by comparing with regular blasthole blasting, was increased by 85.00% in the direction of water jet slot, and the PSPV in the direction perpendicular to the direction of water jet slot was reduced by 70.21%.

(2) In contrast with directional-controlled blasting with water jet assistance, the existence of blasthole wall protection material is not only beneficial to the "guiding effect" of blast-induced crack propagation of water jet slot but also beneficial to reduce blast-induced damage of remaining rock mass.

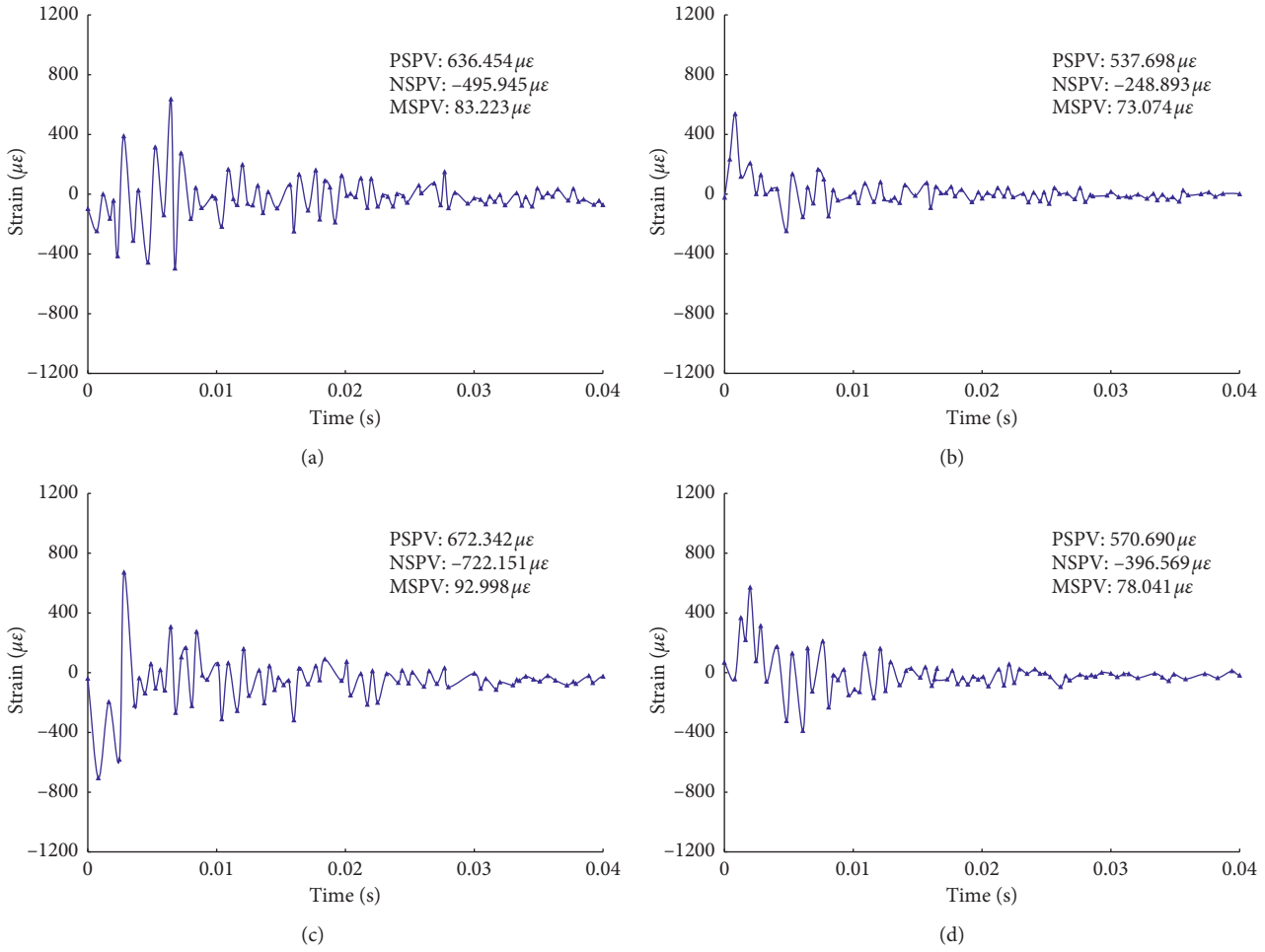

Figure 5: Waveform curve of dynamic strain for #1 test model: (a) #E1-1 test point, (b) #E1-2 test point, (c) #E1-3 test point, and (d) #E1-4 test point.

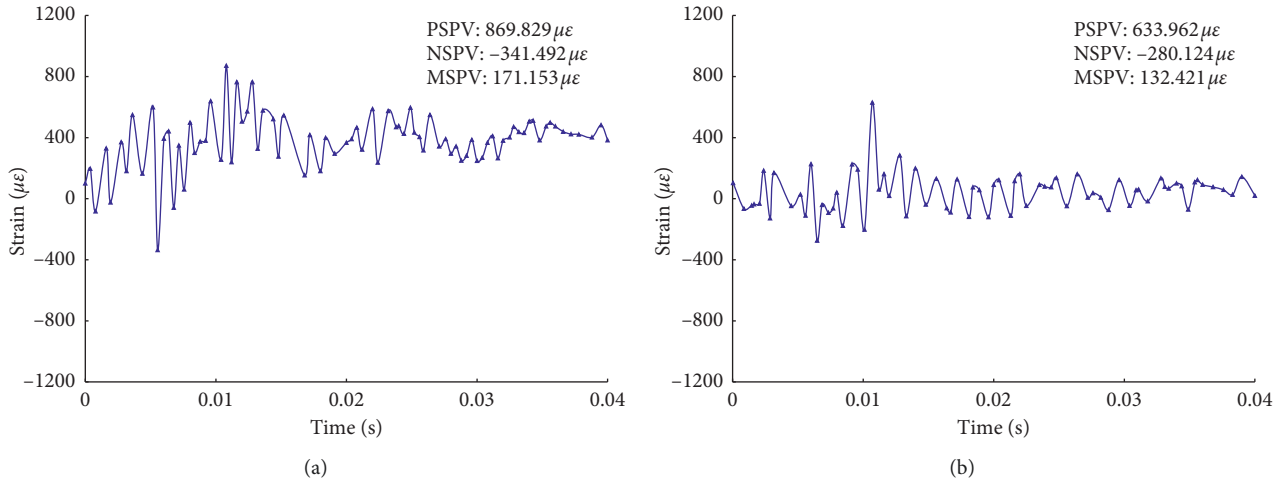

Figure 6: Continued.

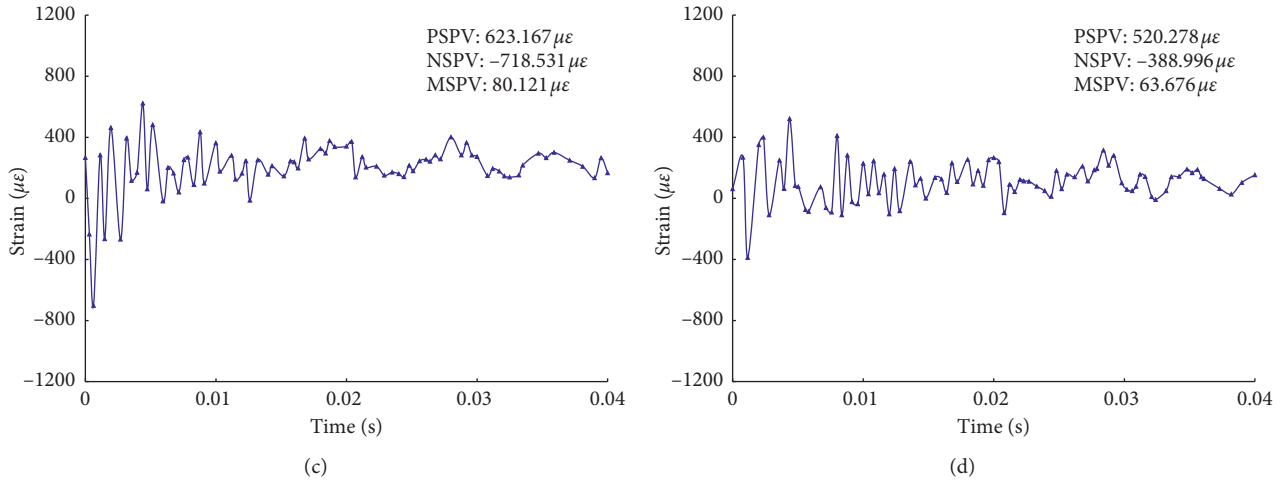

Figure 6: Waveform curve of dynamic strain for #2 test model: (a) #E2-1 test point, (b) #E2-2 test point, (c) #E2-3 test point, and (d) #E2-4 test point.

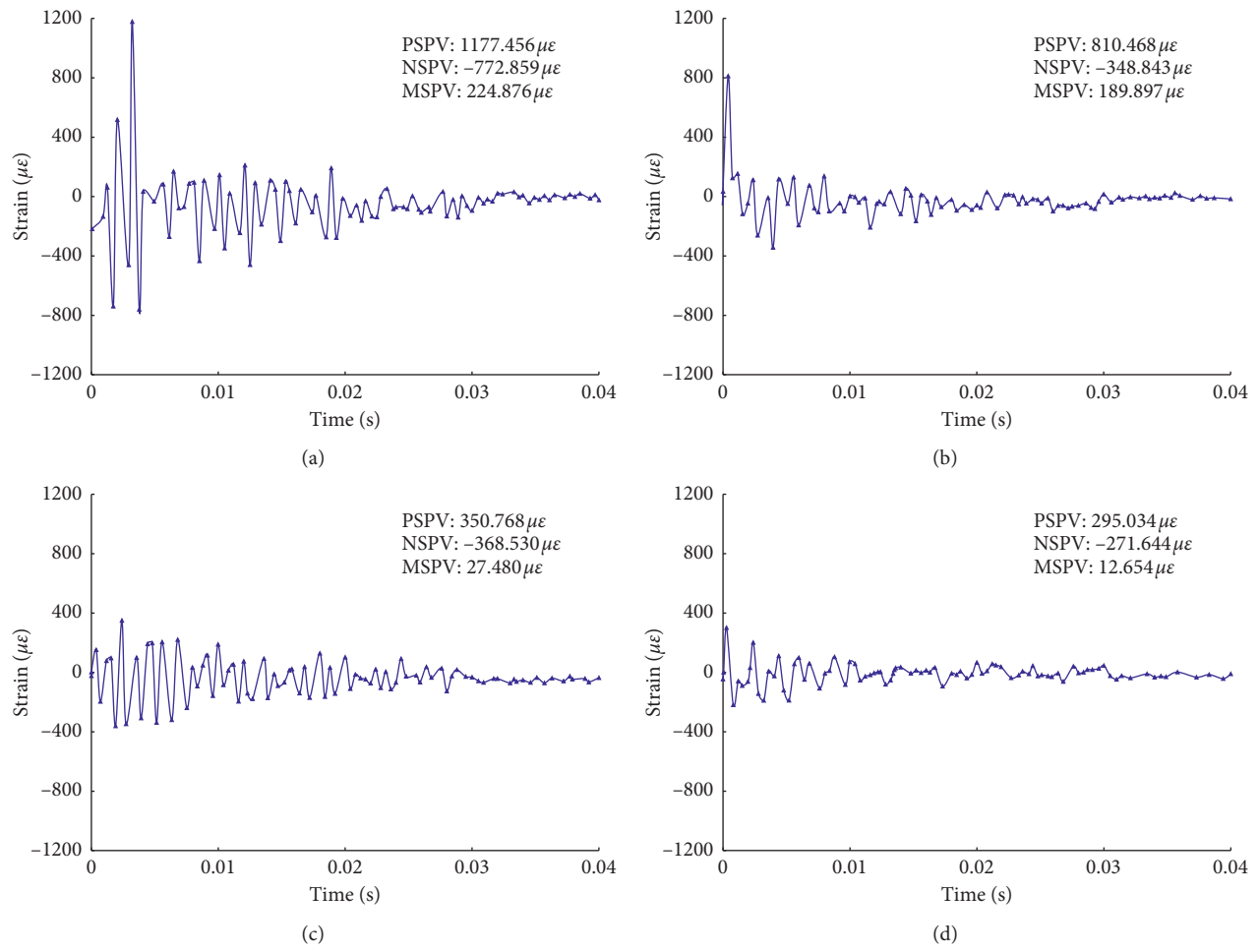

Figure 7: Waveform curve of dynamic strain for #3 test model: (a) #E3-1 test point, (b) #E3-2 test point, (c) #E3-3 test point, and (d) #E3-4 test point.

3. Numerical Simulation of Blast Stress Evolution

The FEM software ANSYS/LS-DYNA and the post-processing software LS-PREPOST were applied to investigate the blasting stress wave evolution law and the blast-induced crack propagation law for different conditions.

3.1. Numerical Simulation Model. Three simulation cases were conducted by ANSYS/LS-DYNA. Due to the symmetry of the simulated object, both simulation cases applied a quasi-2D simulation model. For each case, the size of rock is 150 cm × 150 cm × 0.3 cm, the diameter of blasthole is 5 cm, the thickness of the blasthole wall protection material is 0.5 cm, and the size of the water jet slot is 2.5 cm × 0.5 cm × 0.3 cm. The #3 simulation model is shown in Figure 8.

3.2. Material Model

3.2.1. Rock. Material type #3 of LS-DYNA (*MAT_PLASTIC_KINEMATIC) was applied to model the rock [35], and its parameters are shown in Table 3.

3.2.2. Blasthole Wall Protection Material. Material type #3 of LS-DYNA (*MAT_PLASTIC_KINEMATIC) was applied to model the blasthole wall protection material [35], and its parameters are shown in Table 4.

3.2.3. Explosive. Material type #8 of LS-DYNA (*MAT_HIGH_EXPLOSIVE_BURN) was chosen as the explosive model, and the pressure released by the chemical energy in the engineering calculations was modelled by the Jones–Wilkins–Lee equation of state. The JWL EOS can be written in the following form [35]:

$$P_{\mathrm{e}} = A\left(1-\frac{\omega}{R_1 V}\right)e^{-R_1 V} + B\left(1-\frac{\omega}{R_2 V}\right)e^{-R_2 V} + \frac{\omega E_{\mathrm{e}}}{V}, \quad (1)$$

where P_{e} is the pressure produced by the detonation products from explosive, where ω, A, B, R_1, and R_2 are user-defined input parameters, V is the relative volume, and E_{e} is the internal energy per initial volume, as shown in Table 5.

3.2.4. Air. Air was modelled by the material type #9 of LS-DYNA (*MAT_NULL) with the Gruneisen equation. The pressure P_{a} can be calculated by [35]

$$\begin{cases} P_{\mathrm{a}} = C_0 + C_1\mu + C_2\mu^2 + C_3\mu^3 + \left(C_4 + C_5\mu + C_6\mu^2\right)E_{\mathrm{a}}, \\ \mu = \dfrac{1}{V_{\mathrm{a}}} - 1, \end{cases} \quad (2)$$

where C_0, C_1, C_2, C_3, C_4, C_5, and C_6 are user-defined constants, ρ_{a} is the density of air, V_{a} is the relative volume of air, E_{a} is the internal energy of air, as shown in Table 6.

3.3. Numerical Calculation Algorithm. Lagrange algorithm has the priority of less computation time and accurately describing the boundary movement of structure, so it is always used to analyze the explosive detonation. However, it has a big disadvantage of causing element distortion and even leads to the termination of calculation when dealing with the large deformation numerical calculation. In order to avoid the above problem, fluid-solid coupling algorithm was adopted for the analysis of the explosive detonation, of which, ALE algorithm was used for explosive and air and Lagrange algorithm for rock and protecting pipe. The material derivative equation and the governing equations of the ALE algorithm can be expressed as follows [35]:

$$\begin{aligned} \frac{df(X,t)}{dt} &= \frac{\partial f(\xi,t)}{\partial t} + \left(v_i - w_i\right)\frac{\partial f(x,t)}{\partial x_i}, \\ \frac{\partial \rho}{\partial t} &= \rho\frac{\partial v_i}{\partial x} + \omega_i\frac{\partial \rho}{\partial x}, \\ \rho\frac{\partial v_i}{\partial t} + \rho\omega_i\frac{\partial v_i}{\partial x_j} &= \frac{\partial \sigma_{ij}}{\partial x_j} + \rho f_i, \\ \rho\frac{\partial e}{\partial t} &= \sigma_{ij}\frac{\partial v_i}{\partial x_j} - \frac{\partial q}{\partial x_j} - \rho\omega_i\frac{\partial e}{\partial x_i}, \end{aligned} \quad (3)$$

where f is the physical quantity, v_i is the velocity of particle X, ω_i is the velocity of the computational grid, x_i is the Lagrangian coordinate system, y_i is the Eulerian coordinate system, ρ is the density, v is the particle velocity, e is the internal energy of unit mass, σ_{ij} is the Cauchy stress tensor, f_i is the body force, q_i is the heat flux, and subscripts i and j stand for the direction of coordinate.

At the same time, meshes of explosive and the air were joined with common nodes and so as to rock and protecting pipe. Then, the fluid-solid coupling was defined between the meshes of the explosive, air, rock, and protecting pipe by the keyword. In addition, according to the characteristics of blasting process, the time step of the simulation is 0.67, and the computation time is 0.004 s.

3.4. Simulation Results Analysis. The Postprocessing software LS-PREPOST was used to draw the diagrams of the evolution law of explosion stress wave and crack propagation of different simulation cases, as shown in Figures 9–11.

In general, for regular blasthole blasting, the explosion stress uniformly acts on the wall of blasthole, and the shape of blast stress wave is round, and then the blast-induced crack forms and expands under the blast loading. Due to the characters of blast loading, the gas pressure acting on blasthole wall in all directions can be considered as equivalent, so the well-distributed blast-induced cracks generate near the blasthole, which is consistent with the classical blasting theory.

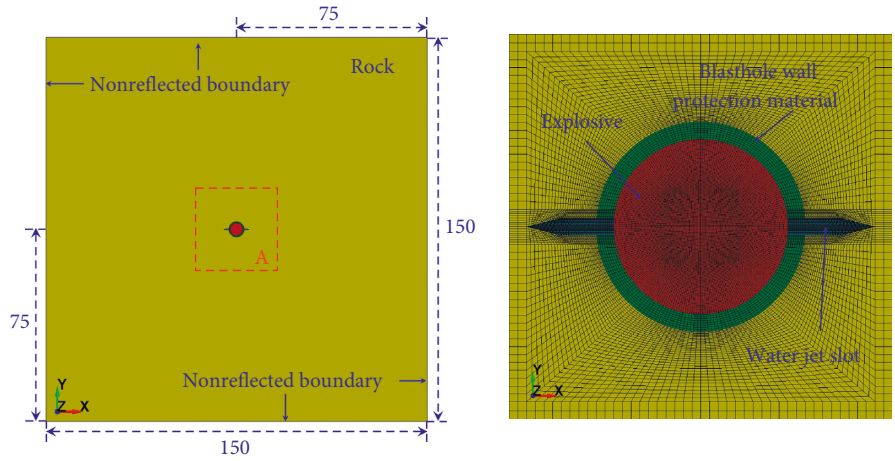

Figure 8: Numerical simulation model: (a) #3 simulation model; (b) enlargement of part A.

Table 3: Parameters of rock.

Density (g/cm^3)	Elastic modulus (MPa)	Tangent modulus (MPa)	Poisson ratio	Yield strength (MPa)	SRC	SRP	Failure strain
2.50	2.25×10^4	4.20×10^3	0.22	3.00	0	0	0.06

Table 4: Parameters of blasthole wall protection material.

Density (g/cm^3)	Elastic modulus (MPa)	Poisson ratio	Yield strength (MPa)	SRC	SRP	Failure strain
1.43	3.00×10^3	0.3	1.8×10^{-1}	0	0	0.1

Table 5: Parameters of explosive and its EOS equation.

ρ_e (g/cm^3)	v_D (cm/μs)	P_{cut} (MPa)	A (MPa)	B (MPa)	R_1	R_2	ω
1.70	0.83	2.95×10^4	8.55×10^5	2.05×10^4	4.60	1.35	0.25

Table 6: Parameters of air and its EOS equation.

ρ_a (g/cm^3)	C_0	C_1	C_2	C_3	C_4	C_5	C_6
1.20×10^{-3}	0.00	0.00	0.00	0.00	0.40	0.40	0.00

However, by comparing #1 simulation case, the blast-induced crack propagation law and the transmission law of explosion stress wave of #2 simulation case and #3 simulation case were greatly changed under the effect of water jet slot and blasthole wall protection materials. On one hand, blasting energy focus forms at the initial stage of the explosion, which promotes the initial microcrack produced at the direction of water jet slot. And nothing but air is in the water jet slot, which caused the formation of low-pressure zone, so detonation products have priority to flow along the direction of water jet slot. Then, the high-pressure and high-velocity gas products wedge into the slot, further leading to crack initiation and extension along the desired direction, as shown in Figures 10 and 11. On the other hand, as the failure of blasthole wall protection material makes a large amount of consumption of blast energy, the formation of microcrack of the remaining rock mass was restrained. Furthermore, the blasthole wall protection material is in a molten state during the blasting, which will wedge into the unexpected microcracks, and then the "gas edge effect" of gas product will be greatly weakened. So, the dual purpose of directional blast-induced crack propagation and remaining rock mass protection is realized.

To further understand the transmission law of blast stress wave and the change regularity of blasting strain under different conditions, monitoring points were set in the numerical simulation model, and its schematic diagram is shown in Figure 12, where D_m stands for the distance between the monitoring point and the center of blasthole, r_b stands for the radius of blasthole, and α_n is the angle between two lines: one is the connection between blasthole center and water jet slot and the another is the connection between blasthole center and monitoring point.

Figures 13–15 show the P-T curves of different simulation cases, from which we can see that with the increase of D_m, the pressure of different cases almost shows a trend of gradual decrease, but the pressure of different monitoring points of different cases shows a different changing trend. For #1 simulation case, when D_m/r_b is certain, each P-T curve shows the same trend because of the explosion. That is because the explosion stress uniformly acts on the wall of blasthole during blasting, which is consistent with experiment test result. For #2 simulation case, when α_n is 0°, the

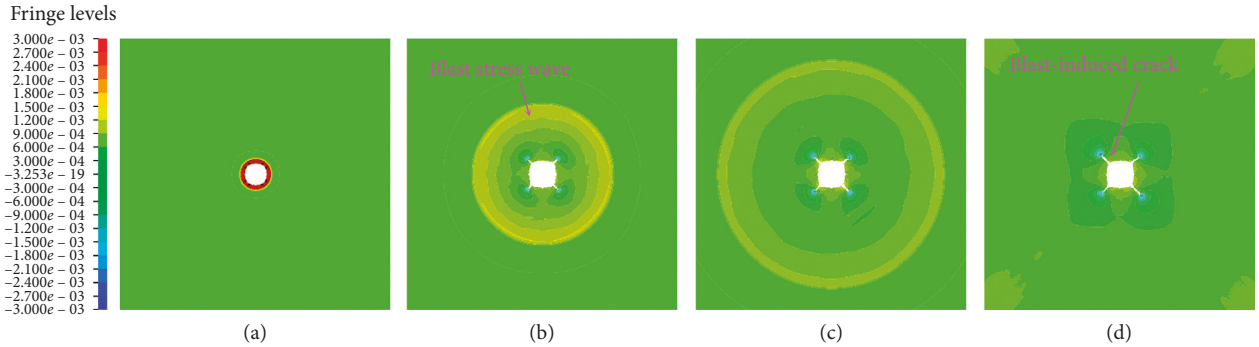

FIGURE 9: Diagram of blast-induced crack propagation and stress wave transmission of #1 simulation case: (a) $t = 20\,\mu s$, (b) $t = 120\,\mu s$, (c) $t = 240\,\mu s$, and (d) $t = 460\,\mu s$.

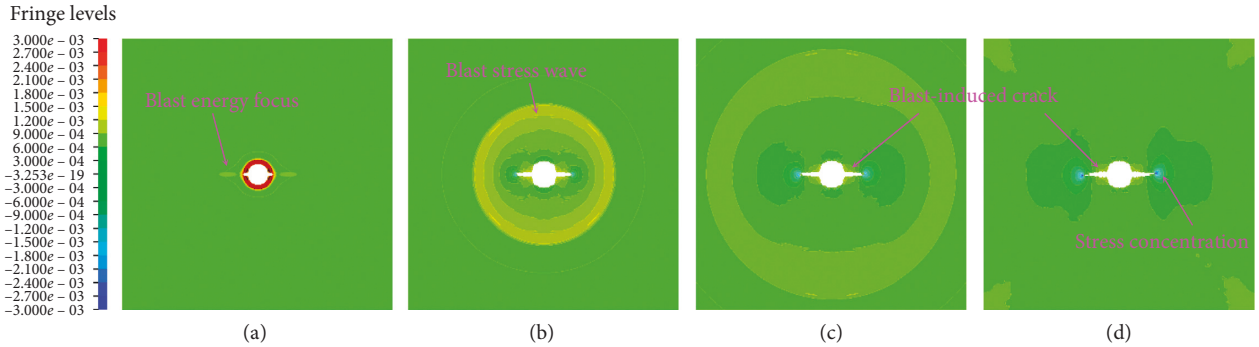

FIGURE 10: Diagram of blast-induced crack propagation and stress wave transmission of #2 simulation case: (a) $t = 20\,\mu s$, (b) $t = 120\,\mu s$, (c) $t = 240\,\mu s$, and (d) $t = 460\,\mu s$.

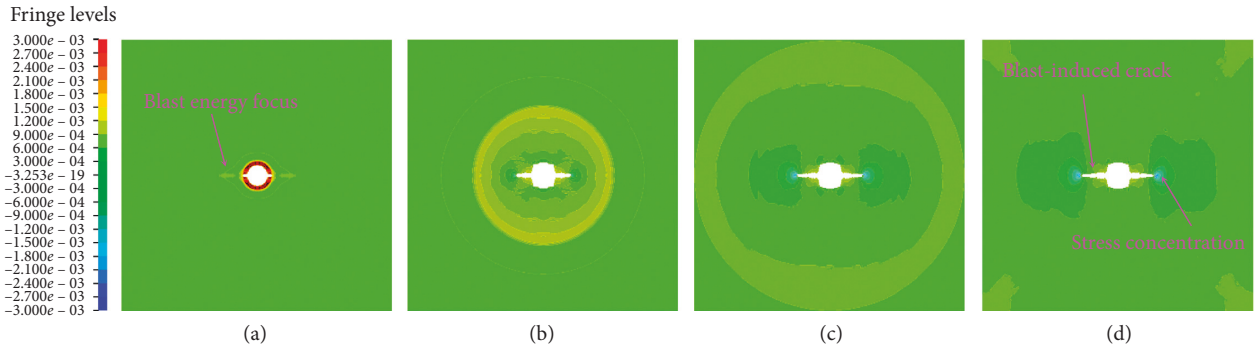

FIGURE 11: Diagram of blast-induced crack propagation and stress wave transmission of #3 simulation case: (a) $t = 20\,\mu s$, (b) $t = 120\,\mu s$, (c) $t = 240\,\mu s$, and (d) $t = 460\,\mu s$.

peak value of the measuring point is smaller than that of regular blasting, but the valley value is bigger than that of regular blasthole blasting. That is to say, the rock will be subjected to tensile stress. As we know, the tensile strength of rock is far less than its compressive strength, so the rock is vulnerable to failure [34], which suggest that the existence of the water jet slot changed the distribution laws of stress fields during blasting, let the blast-induced crack initiation and propagation in the direction of water jet slot.

For #3 simulation case, when α_n is 0°, though the peak value continues to decline, valley value is 40.40% greater than that of #2 simulation case. Moreover, the action time of tensile stress of #3 simulation case is much longer than that of #2 simulation case. When α_n is 90°, the peak value is 25.34% and 29.66% smaller than that of #2 simulation case and #1 simulation case, respectively, which demonstrates that the existence of blasthole wall protection material has created more favorable conditions for the blast-induced crack propagation along the direction of water jet slot and the protection of blasthole wall during blasting, which is consistent with the above analysis.

Figures 16–18 present the effective stress curves of different simulation cases. For #1 simulation case, as the explosion stress uniformly acts on the wall of blasthole during

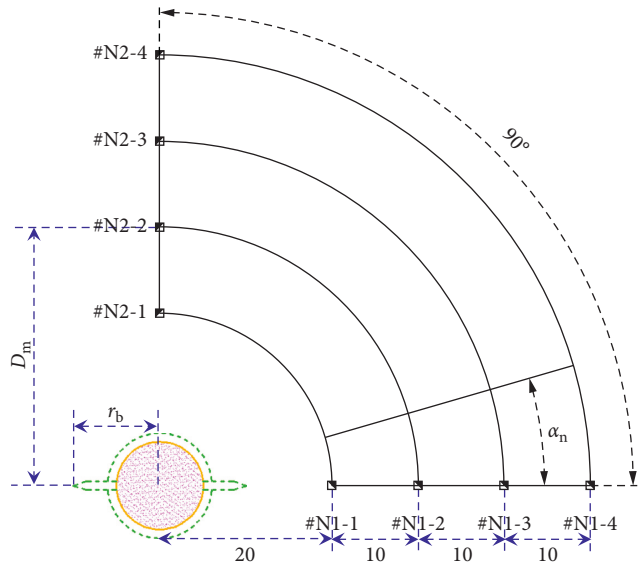

Figure 12: Schematic diagram of monitoring point layout.

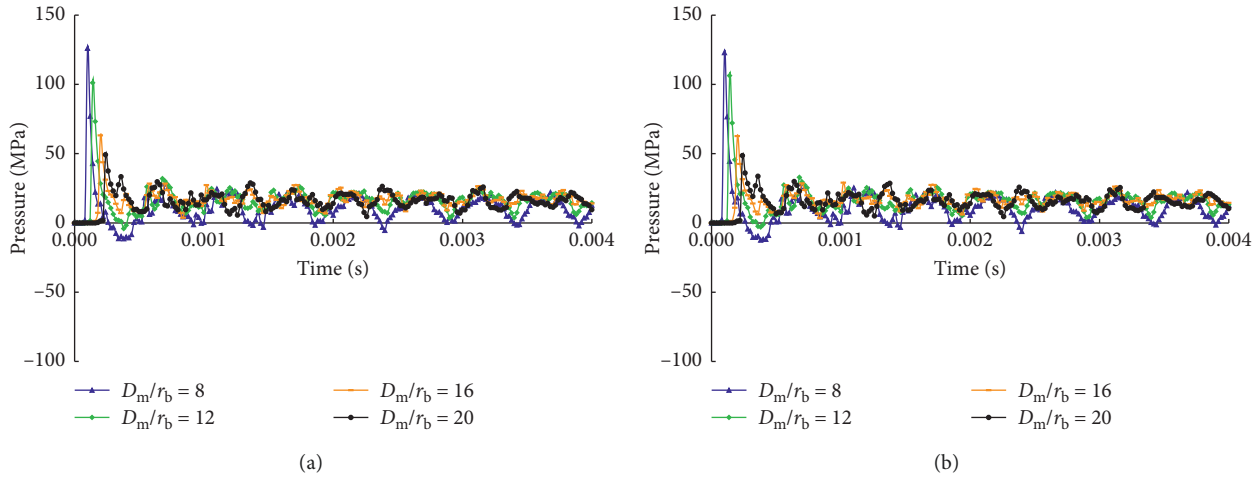

Figure 13: P-T curve of different monitoring points of #1 simulation case: (a) $\alpha_n = 0^\circ$; (b) $\alpha_n = 90^\circ$.

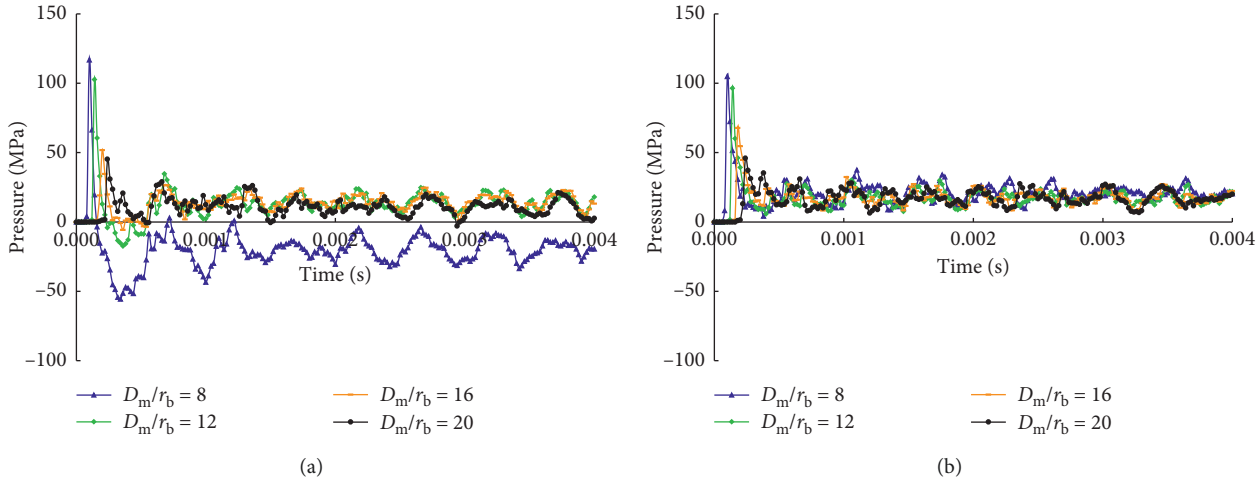

Figure 14: P-T curve of different monitoring points of #2 simulation case: (a) $\alpha_n = 0^\circ$; (b) $\alpha_n = 90^\circ$.

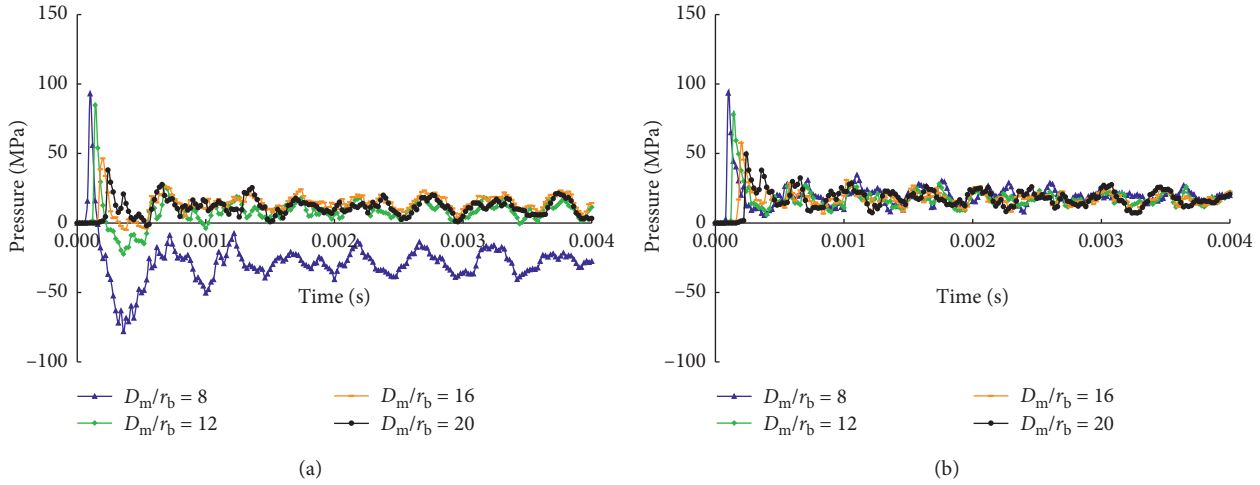

Figure 15: P-T curve of different monitoring points of #3 simulation case: (a) $\alpha_n = 0^\circ$; (b) $\alpha_n = 90^\circ$.

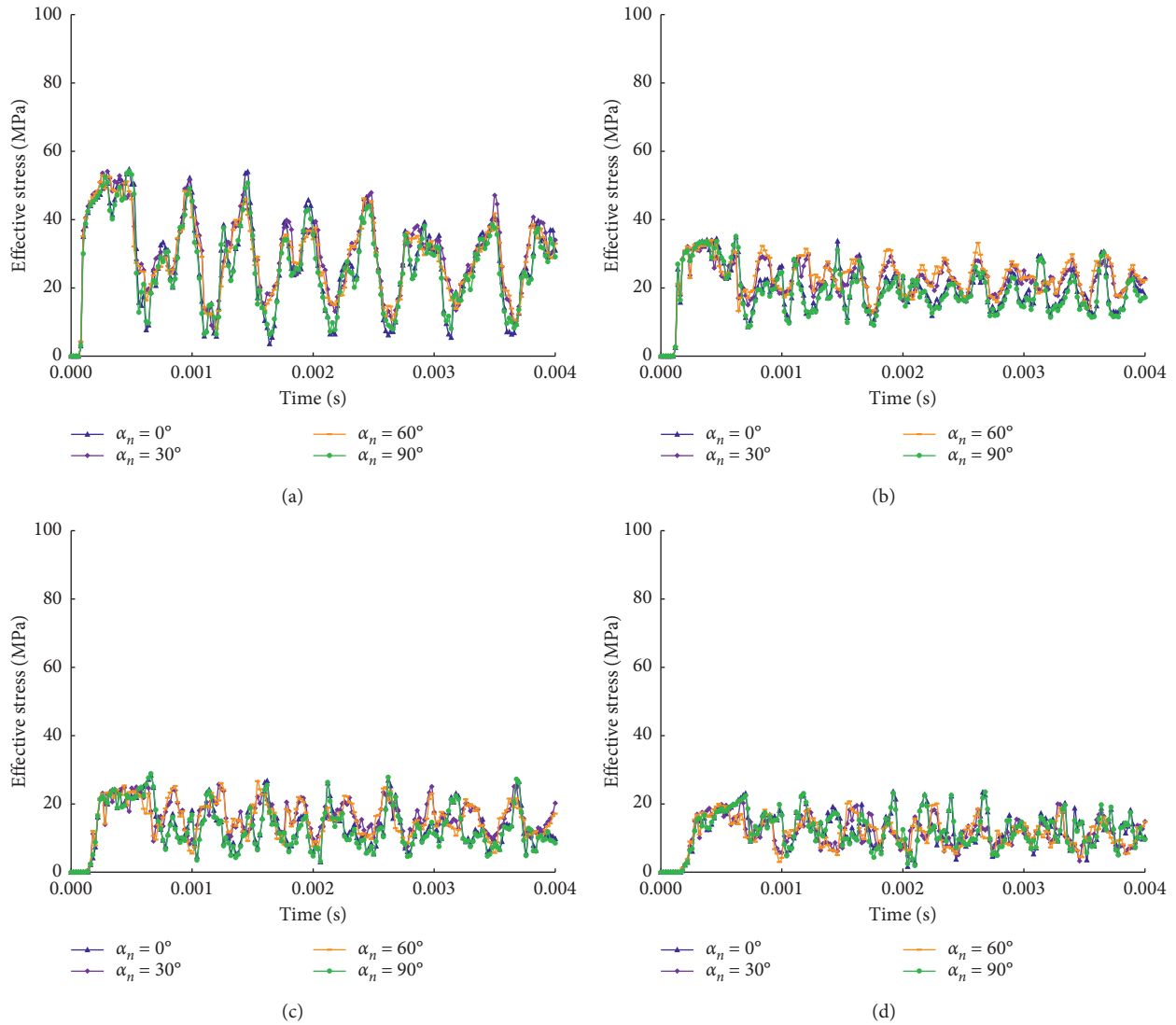

Figure 16: Effective stress curve of different monitoring points of #1 simulation case. (a) $D_m/r_b = 8$. (b) $D_m/r_b = 12$. (c) $D_m/r_b = 16$. (d) $D_m/r_b = 20$.

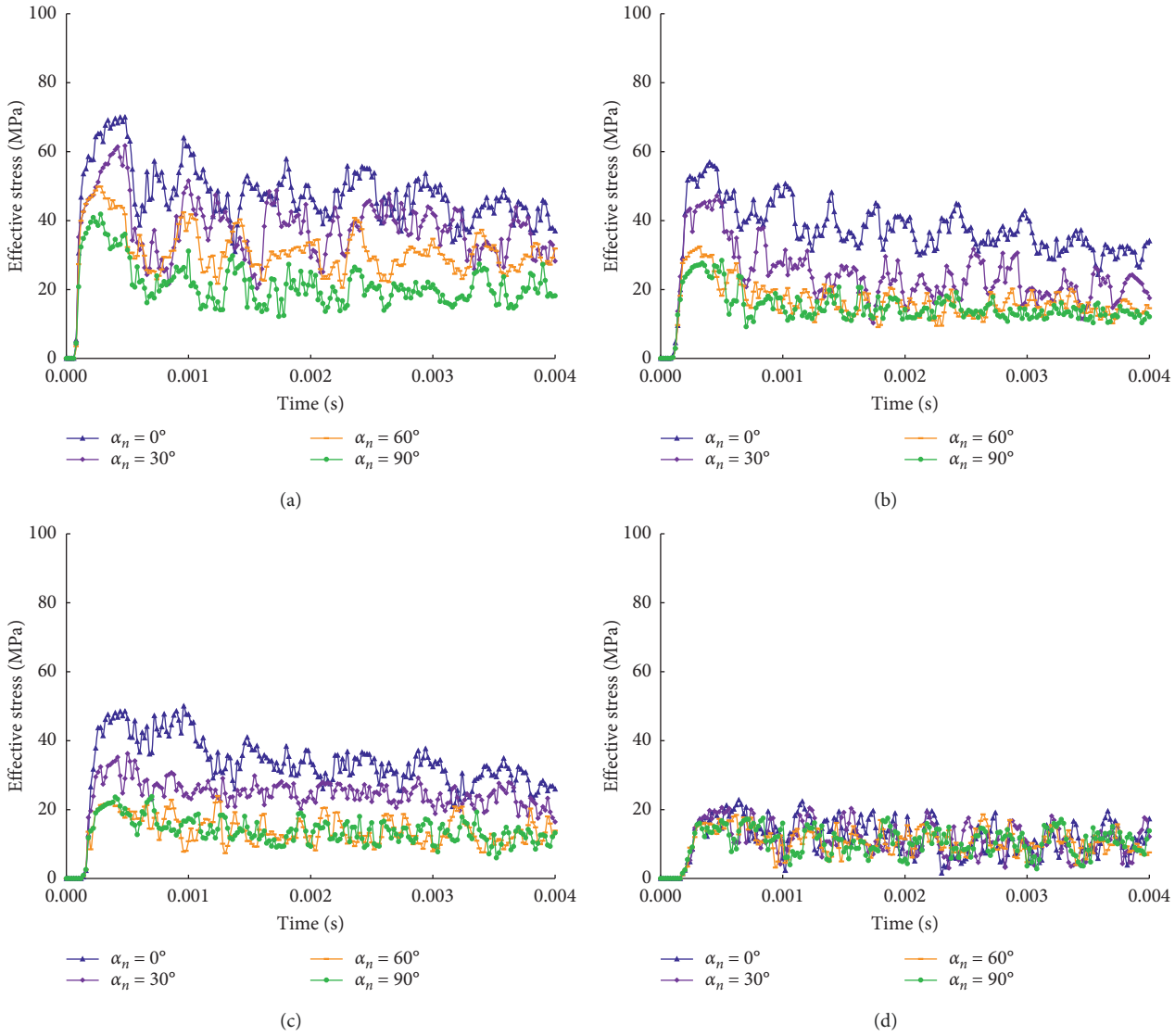

FIGURE 17: Effective stress curve of different monitoring points of #2 simulation case. (a) $D_m/r_b = 8$. (b) $D_m/r_b = 12$. (c) $D_m/r_b = 16$. (d) $D_m/r_b = 20$.

blasting, the effective stress of each curve shows the same trend if D_m/r_b is certain, and the effective stress decreases gradually and becomes stable with the increase of D_m/r_b. For #2 simulation case, the peak value of effective stress decreases with the increase of D_m/r_b and α_n. That is to say, if D_m/r_b is certain, the rock located at different directions around the blasthole suffered different effective stress; the closer the rock gets to the direction of water jet, the bigger the effective stress the rock suffered. For #3 simulation case, the variation trend of effective stress is similar to that of #2 simulation case, but the peak value of each effective stress curve is quite different. By comparing each effective stress curve of #2 simulation case and #3 simulation case, we can see that in the direction of water jet slot, the peak value of effective stress of #3 simulation case is always bigger than that of #2 simulation case. However, in the direction perpendicular to the direction of the jet slot, the peak value of effective stress of #3 simulation case is always smaller than that of #2 simulation case, which indicates that the existence of blasthole wall protection material is not only very beneficial to the "guiding effect" of blast-induced crack propagation by water jet slot but also beneficial to reduce blast-induced damage of remaining rock mass.

Moreover, by comparing Figures 16(d), 17(d), and 18(d), we can see that in the direction of water jet slot, the effective stress of #2 simulation case decreases gradually, and when D_m/r_b is 20, the distribution-evolution law of effective stress is similar to that of #1 simulation case. However, for #3 simulation case, when D_m/r_b is 20, the peak value of effective stress is bigger than that of #2 simulation case and the growing trend of effective stress shows a large fluctuation, which suggested that the rock suffered the "guiding effect" by water jet slot. In addition, in the other direction of blasthole, the distribution-evolution law of effective stress is similar to that of #1 simulation case. That is to say, the bigger D_m/r_b is, the weaker the "guiding effect" and "blasthole wall

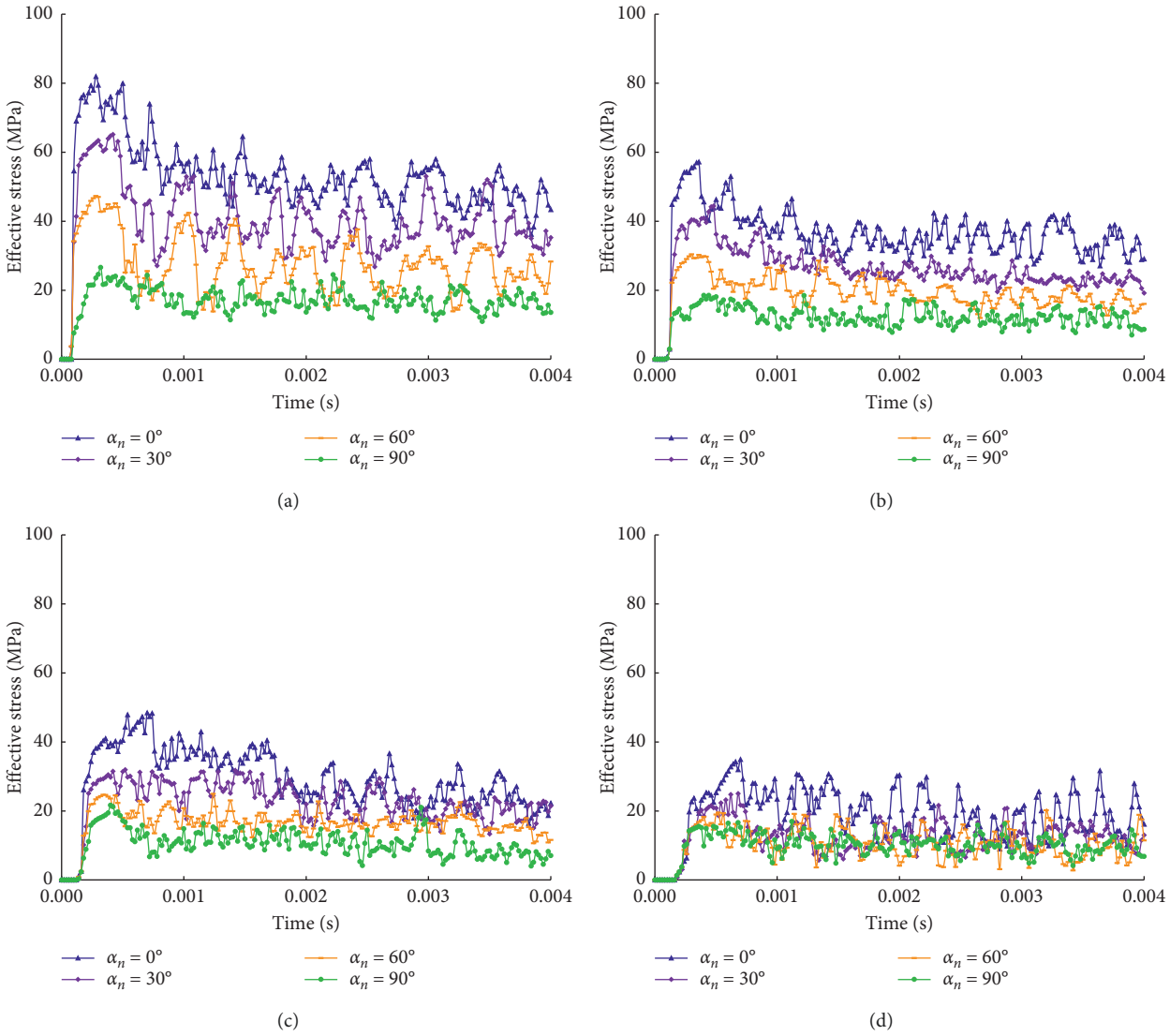

Figure 18: Effective stress curve of different monitoring points of #3 simulation case. (a) $D_m/r_b = 8$. (b) $D_m/r_b = 12$. (c) $D_m/r_b = 16$. (d) $D_m/r_b = 20$.

protection effect" by water jet slot and wall protection material are.

4. Conclusions

In summary, some conclusions can be summarized as follows.

The experiment test on dynamic blast strain was conducted, and the results indicated that under the combined effect of blasthole wall protection material and water jet slot, the blasting strain fields were changed by comparing with the regular blasthole blasting. In the direction of water jet slot, the PSPV was increased by 85.00%, and in the direction perpendicular to the direction of water jet slot, the PSPV was reduced by 70.21%.

Numerical simulation results suggest that the existence of water jet slot and blasthole wall protection material can affect the distribution and evolution law of explosive stress wave and let the stress concentration occur at the tip of water jet slot, which promotes blast-induced crack propagation along the specific direction and minimizes the blast-induced damage of remaining rock mass. Moreover, the bigger D_m/r_b is, the weaker the "guiding effect" and "blasthole wall protection effect" by water jet slot and wall protection material are.

Both the experiment test result and the numerical simulation results indicated that the existence of blasthole wall protection material is not only beneficial to the "guiding effect" of blast-induced crack propagation of water jet slot but also beneficial to reduce blast-induced damage of remaining rock mass.

Future research work will be focused on the applications in practical engineering of this approach.

Data Availability

Readers can access the data supporting the conclusions of the study by sending a mail to the corresponding author

(e-mail: dengfengcqu@163.com), and all data can be cosh-ared without restriction.

Conflicts of Interest

The authors declare that they have no conflicts of interest.

Acknowledgments

Financial support for this work was provided by the Natural Science Foundation of Southwest University of Science and Technology (18zx7124). In particular, the authors thank M. E. D. Y. Li and M. E. F. W. Yan for their kind help in experimental investigation and sincere suggestion.

References

[1] Z. N. Zhao, X. T. Feng, Y. X. Xiao et al., "Microseismic characteristics and rockburst risk of deep tunnel constructed by different excavation methods," *Chinese Journal of Geotechnical Engineering*, vol. 38, no. 5, pp. 0867–0876, 2016.

[2] Z. C. Zhang, "Control in blasting engineering," *Chinese Journal of Underground Space and Engineering*, vol. 9, no. 5, pp. 1208–1214, 2013.

[3] Y. Wang, "Study of the dynamic fracture effect using slotted cartridge decoupling charge blasting," *International Journal of Rock Mechanics and Mining Sciences*, vol. 96, pp. 34–46, 2017.

[4] S. S. Rathore and S. Bhandari, "Controlled fracture growth by blasting while protecting damages to remaining rock," *Rock Mechanics and Rock Engineering*, vol. 40, no. 3, pp. 317–326, 2007.

[5] S. H. Cho, Y. Nakamura, B. Mohanty, H. S. Yang, and K. Kaneko, "Numerical study of fracture plane control in laboratory-scale blasting," *Engineering Fracture Mechanics*, vol. 75, no. 13, pp. 3966–3984, 2008.

[6] R. S. Yang, Y. B. Wang, and L. Y. Yang, "Dynamic caustic experimental study of crack propagation in two borehole cut blasting," *Journal of China University of Mining & Technology*, vol. 41, no. 6, pp. 868–872, 2012.

[7] W. M. Liang, X. L. Yang, and Y. Q. Yu, "Research on theory on directional fracture controlled blasting," *Journal of Liaoning Technical University*, vol. 25, no. 5, pp. 702–704, 2006.

[8] J. S. Song, Y. B. Wang, X. T. Gao et al., "The mechanism of directional fracture controlled blasting and its application," *Journal of Mining Science and Technology*, vol. 1, no. 1, pp. 16–28, 2016.

[9] Y. Wang, "Experimental research on the influence of an empty-hole defect on crack connections between a directionally fractured blast hole," *Journal of Testing and Evaluation*, vol. 45, no. 6, pp. 2139–2150, 2017.

[10] Z. Li, W. Chen, and H. Hao, "Numerical study of sandwich panel with a new bi-directional load-self-cancelling (LSC) core under blast loading," *Thin-Walled Structures*, vol. 127, pp. 90–101, 2018.

[11] K. Katsuyama, H. Kiyokawa, and K. Sassa, "Control the growth of cracks from a borehole by a new method of smooth blasting," *Mining Safety*, vol. 29, pp. 16–23, 1983.

[12] W. L. Fourney, D. B. Barker, and D. C. Holloway, "Model studies of explosive well stimulation techniques," *International Journal of Rock Mechanics and Mining Sciences & Geomechanics Abstracts*, vol. 18, no. 2, pp. 113–127, 1981.

[13] W. L. Fourney, D. B. Barker, and D. C. Holloway, "Model studies of well stimulation using propellant charges," *International Journal of Rock Mechanics and Mining Sciences & Geomechanics Abstracts*, vol. 20, no. 2, pp. 91–101, 1983.

[14] B. Mohanty, "Explosive generated fractures in rock and rock like materials," *Engineering Fracture Mechanics*, vol. 35, no. 4-5, pp. 889–898, 1990.

[15] B. Mohanty, "Fracture-plane control blasts with satellite holes," in *Proceedings of 3rd International Symposium on Rock Fragmentation by Blasting*, pp. 407–418, Australasian Institute of Mining and Metallurgy, Parkville, Australia, August 1990.

[16] Y. G. Du, Z. C. Zhang, and T. L. Li, "Studies on mechanical effect produced by the V-shaped notch borehole blasting," *Explosion and Shock Waves*, vol. 11, pp. 26–30, 1991.

[17] Q. Zong, "Theoretical study on the cracking mechanism of notched borehole blasting," *Coal Mine Blasting*, vol. 1, pp. 12–16, 1995.

[18] Q. Zong, "Investigations into mechanism of crack formation for grooved hole-well blasting," *Chinese Journal of Geotechnical Engineering*, vol. 20, no. 1, pp. 30–33, 1998.

[19] S. H. Cho, Y. Nakamura, and K. Kaneko, "Dynamic fracture process analysis of rock subjected to a stress wave and gas pressurization," *International Journal of Rock Mechanics and Mining Sciences*, vol. 41, no. 3, pp. 433–440, 2004.

[20] Y. Zhang, "Dynamic numerical simulation for the mechanism of V-shaped notch blasting," *Explosive Materials*, vol. 38, no. 4, pp. 1–5, 2009.

[21] R. S. Yang and Y. B. Wang, "Dynamic caustic experiment on fracture behaviors of flawed material induced by pre-notched blasting," *Explosive and Shock Waves*, vol. 36, no. 2, pp. 145–152, 2016.

[22] R. S. Yang, C. X. Ding, L. Y. Yang, P. Xu, and C. Chen, "Hole defects affect the dynamic fracture behavior of nearby running cracks," *Shock and Vibration*, vol. 2018, Article ID 5894356, 8 pages, 2018.

[23] Z. W. Yue, Y. Guo, X. Wang et al., "Influence of empty hole shape on directional fracture controlled blasting of rock," *Rock and Soil Mechanics*, vol. 37, no. 2, pp. 376–382, 2016.

[24] Z. Yue, P. Qiu, R. Yang, S. Zhang, K. Yuan, and Z. Li, "Stress analysis of the interaction of a running crack and blasting waves by caustics method," *Engineering Fracture Mechanics*, vol. 184, pp. 339–351, 2017.

[25] B. Chen, C. Liu, and J. X. Yang, "Analysis and application on controlling thick hard roof caving with deep-hole position presplitting blasting," *Advances in Civil Engineering*, vol. 2018, Article ID 9763137, 15 pages, 2018.

[26] Y. H. Zhu and X. P. Xu, "Damage control characteristics for notched blasting based on the damage mechanism," *Journal of China Coal Society*, vol. 42, no. 2, pp. 369–376, 2017.

[27] X. H. Li, L. Yang, J. S. Wang et al., "The natural frequency characteristic of the self-excited oscillation pulsed water jet device," *Journal of China Coal Society*, vol. 25, no. 6, pp. 641–644, 2000.

[28] X. H. Li, Y. Y. Lu, Y. Zhao et al., "Study on improving the permeability of soft coal seam with high pressure pulsed water jet," *Journal of China Coal Society*, vol. 33, no. 12, pp. 1386–1390, 2007.

[29] Y. Kang, X. C. Wang, X. F. Yang et al., "Numerical simulation of control blasting with borehole protecting and water jet slotting in soft rock mass," *Disaster Advances*, vol. 5, no. 4, pp. 933–938, 2012.

[30] J.-G. Kim and J.-J. Song, "Abrasive water jet cutting methods for reducing blast-induced ground vibration in tunnel excavation," *International Journal of Rock Mechanics and Mining Sciences*, vol. 75, pp. 147–158, 2015.

[31] Y. Kang, D. D. Zheng, D. F. Su et al., "Model of directional shaped blasting assisted with water jet and its numerical simulation," *Journal of Vibration and Shock*, vol. 34, pp. 182–188, 2015.
[32] D. Su, Y. Kang, F. Yan, D. Zheng, X. Wang, and M. Wei, "Crack propagation law affected by natural fracture and water jet slot under blast loading," *Combustion, Explosion, and Shock Waves*, vol. 54, no. 6, pp. 747–756, 2018.
[33] Y. B. Wang, "Rock dynamic fracture characteristics based on NSCB impact method," *Shock and Vibration*, vol. 2018, Article ID 3105384, 13 pages, 2018.
[34] J. Dai, *Dynamic Behaviors and Blasting Theory of Rock*, Metallurgical Industry Press, Beijing, China, 2013.
[35] LSTC, *LS-DYNA Keyword User's Manual*, Livermore Software Technology Corporation, Livermore, CA, USA, 2007.